RAPID COMMUNICATIONS

PHYSICAL REVIEW C VOLUME 45, NUMBER 6 JUNE 1992

Analyzing power measurements for p-d radiative capture

F. Goeckner,* W. K. Pitts, and L. D. Knutson
University of Wisconsin, Madison, Wisconsin 53706
(Received 6 March 1992)

Analyzing power measurements are presented for radiative capture of polarized protons on deuterium and for polarized deuterons on hydrogen at $E_{\text{c.m.}}=3.33$ MeV. The reaction is dominated by $E1$ capture from channel-spin $S_c=\frac{1}{2}$ states; however, the measurements show clear evidence of $M1$, $E2$, and spin-flip ($S_c=\frac{3}{2}$) $E1$ contributions at the $\frac{1}{2}$% level. The new data can impose fairly strong constraints on individual matrix elements.

PACS number(s): 25.10.+s, 24.70.+s

The three-nucleon system plays a unique role in the study of the properties of nuclei. Clearly, one of the fundamental questions in nuclear physics is whether we can understand the nature of complex nuclear systems using potentials derived from nucleon-nucleon experiments. In complex multinucleon systems, the answer to this question is generally obscured by the fact that theoretical calculations inevitably involve the use of simplifying approximations, often of questionable validity. For the three-nucleon system the situation is quite different. In this case the theory has advanced to a point where, for many situations, it is possible to find solutions of the Schrödinger equation which are essentially exact in the mathematical sense. The result is that when a discrepancy arises between theory and experiment, it indicates a failure of the basic theoretical assumptions (e.g., a problem with the assumed N-N interaction, the existence of many-body forces, etc.).

In this paper we present new measurements of the cross section and polarization observables for proton-deuteron radiative capture. In particular we have measured angular distributions of the differential cross section and analyzing power, A_y, for capture of polarized protons on deuterium at $E_p=5$ MeV ($E_{\text{c.m.}}=3.33$ MeV). In addition, we have measured the vector and tensor analyzing powers, iT_{11}, T_{20}, T_{21}, and T_{22}, for capture of polarized deuterons on hydrogen at the corresponding energy, $E_d=10$ MeV. Our goal in undertaking this experiment was primarily to provide a high-quality data set for testing various theoretical calculations of p-d radiative capture, which in turn may ultimately lead to a deeper understanding of the strong interaction. In addition, as we shall show below, the measurements by themselves provide a good deal of valuable information concerning the nature of the capture reaction.

The measurements were carried out at the University of Wisconsin tandem accelerator laboratory using proton and deuteron beams from the crossed-beam polarized ion source [1]. The accelerated beam was used to bombard gas targets of either deuterium or hydrogen. Gamma rays from the capture reactions were detected with a shielded, Compton suppressed 25 cm by 25 cm NaI detector [2].

In order to eliminate backgrounds arising from capture of slow neutrons in the NaI crystal and the surrounding material, the polarized beam was bunched and chopped at a frequency of either 7.4 or 5.2 MHz, and the timing of the γ-ray signal relative to the buncher rf was measured for each event. The timing peak had a full width at half maximum of typically 5 ns. Most of the thermal neutron background was eliminated by accepting only events within a narrow window on the peak, and the remaining background was subtracted using "accidentals" spectra constructed from events lying on either side of the peak.

The target cell used for the measurements of σ and A_y was 3.65 cm in diameter. The beam entrance and exit windows consisted of 2.5-μm-thick W foils, and the cell pressure was typically 213 kPa. For the measurements that involved using the polarized deuteron beam a more elaborate arrangement was required, primarily because backgrounds from neutrons and γ rays produced in the entrance and exit foils of the cell were sufficiently intense to obscure the peak of interest. The target cell used for these measurements consisted of a 14-cm-long tube oriented coaxially with the beam, with entrance and exit foils (4-μm and 6-μm Ta, respectively) epoxied onto curved surfaces at either end of the tube. The typical operating pressure was 304 kPa. Carefully machined shadow blocks fabricated from a machinable tungsten alloy were used to shield the NaI detector from radiation produced in the foils. The blocks for each angle were designed so that the NaI detector could view a region 4 cm long at the center of the cell. In order to increase the counting rate and the signal to background ratio, both cells were fixed to the bottom of a liquid nitrogen bath, with a resulting operating temperature of around 90 K.

Because of the complex geometry used for the deuteron-beam measurements, the relative differential cross sections were extracted from the proton-beam measurements only. No attempt was made to determine the absolute scale of the differential cross sections.

In Fig. 1 we show γ-ray spectra for the proton-beam measurements at laboratory angles of 25° and 155°, where the cross section is smallest. The plots show the number of counts as a function of γ-ray energy after subtraction of the random "accidental" background. The

*Present address: Department of Physics, Ohio University, Athens, OH 45701.

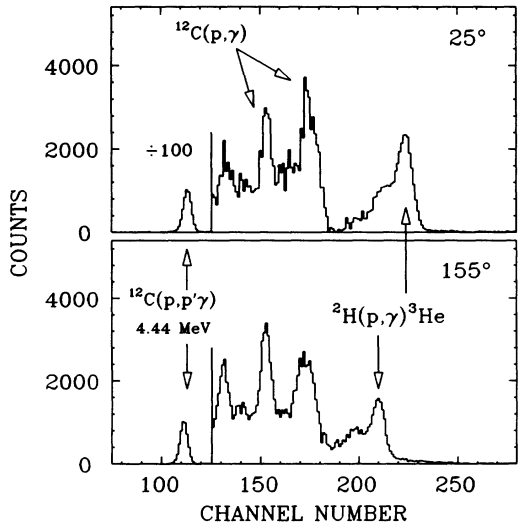

FIG. 1. NaI pulse-height spectra for radiative capture of protons on deuterium at $E_p = 5$ MeV. The dispersion is approximately 40 keV/channel. Counts from random background have been removed by imposing a cut on the arrival time of the γ ray relative to the buncher rf. The remaining background events were subtracted using "accidentals" spectra. The counts below the p-d capture peak arise primarily from reactions on the ^{12}C deposits on the entrance and exit foils of the gas cell.

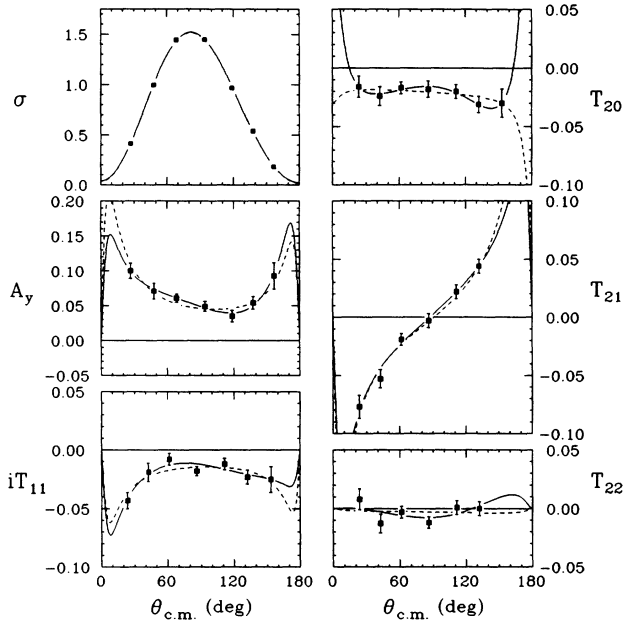

FIG. 2. Measurements of the cross section and analyzing powers for p-d radiative capture at $E_{c.m.} = 3.33$ MeV. The solid curves show the best Legendre polynomial fit, while the dashed curves are a matrix element fit corresponding to the parameters of Table IV.

capture peaks have the expected shape, consisting of a prominent total energy peak with a shoulder resulting from single and double escape. The relative differential cross sections were extracted by fitting the observed spectra using peak shapes with all parameters fixed from angle to angle except for the peak position and intensity. For the deuteron-beam measurements, the peaks were less cleanly separated from the background. However, the measured background asymmetries were small, and consequently the spectra were still quite adequate for the determination of the analyzing powers.

The analyzing powers were measured using fast spin flipping cycles in which the polarization was reversed each 0.25 s. For the deuteron tensor analyzing powers, the spin switching cycle consisted of four states including all combinations of positive and negative vector and tensor polarization. To minimize error propagation in the determination of the tensor analyzing powers, measurements were taken for a total of five different orientations of the spin quantization axis, chosen in such a way that each analyzing power could essentially be determined independently of the others. Further experimental details are given in Ref. [3].

A series of Monte Carlo calculations was carried out for each target cell to determine corrections for finite geometry and gamma-ray attenuation effects. These corrections are significant only for the cross-section measurements, and in this case turn out to be as large as 2.5 times the quoted experimental errors. However, all the important geometrical effects are well understood, and consequently the resulting uncertainties are negligible.

The new measurements are shown in Fig. 2. In all of the graphs, θ represents the angle (in the c.m.) between the incident proton and the outgoing γ ray. The error bars displayed in the figure incorporate all significant sources of error, including statistics, background subtraction and peakfitting, uncertainties in the deadtime corrections and in the density and location of the target, and the uncertainty associated with measurement of the beam polarization. Numerical data tables are available from the authors on request.

The present experiment represents the first time that measurements of all the analyzing powers have been obtained at a single energy. There have been several previous measurements of A_y at low energies [4–7]. In addition, there are reasonably accurate measurements of iT_{11} at $E_{c.m.} = 2.0$ and 31.5 MeV [7,8] and of either T_{20} or the related parameter A_{yy} at 6.6, 9.2, 9.7, 15.1, and 31.5 MeV [8–11]. The data shown in Fig. 2 represent the first measurement of T_{21}, which, as one can see, is the largest deuteron analyzing power.

We now address the question of what these measurements reveal about the nature of the capture reaction. From general arguments one expects the reaction to be dominated by $E1$ radiation, with relatively small contributions from $M1$ and $E2$. The allowed $E1$, $E2$, and $M1$ matrix elements are listed in Table I in the usual spectroscopic notation. In the ^{3}He bound state wave function the spin quantum number is predominantly $S = \frac{1}{2}$, and consequently one expects that, for the electric multipoles, the reaction matrix elements for the doublet states (channel spin $S_c = \frac{1}{2}$) will be significantly larger than for the quartet ($S_c = \frac{3}{2}$) states. It is well known, however, that if the $S_c = \frac{3}{2}$ states do not contribute to the reaction, then the deuteron tensor analyzing powers (T_{20}, T_{21}, and T_{22}) will

TABLE I. Allowed $E1$, $M1$, and $E2$ transition matrix elements for p-d radiative capture. The quantity S_c is the channel spin, $\mathbf{S}_c = \mathbf{S}_p + \mathbf{S}_d$.

	$S_c = \frac{1}{2}$	$S_c = \frac{3}{2}$
$E1$	$^2P_{1/2}$ $^2P_{3/2}$	$^4P_{1/2}$ $^4P_{3/2}$ $^4F_{3/2}$
$M1$	$^2S_{1/2}$ $^2D_{3/2}$	$^4S_{3/2}$ $^4D_{1/2}$ $^4D_{3/2}$
$E2$	$^2D_{3/2}$ $^2D_{5/2}$	$^4S_{3/2}$ $^4S_{3/2}$ $^4D_{5/2}$ $^4G_{5/2}$

be identically zero. Thus, it is evident from the measurements that the $S_c = \frac{3}{2}$ ("spin-flip") transitions contribute at least to some extent. These spin-flip transitions can arise either from D-state components in the ^{3}He wave function, or alternatively from the deuteron D state or from channel-spin mixing in the scattering states.

One can extract more detailed information about the various multipole contributions to the reaction by expanding the data in terms of Legendre functions. The formulas we use are the following [12,13]:

$$\sigma(\theta) = A_0 \left[1 + \sum_{l=1}^{4} a_l P_l(\cos\theta) \right], \tag{1}$$

$$\sigma(\theta) A_y(\theta) = A_0 \sum_{l=1}^{4} b_l P_l^1(\cos\theta), \tag{2}$$

$$\sigma(\theta) iT_{11}(\theta) = \frac{A_0}{\sqrt{3}} \sum_{l=1}^{4} b_l' P_l^1(\cos\theta), \tag{3}$$

$$\sigma(\theta) T_{20}(\theta) = A_0 \sum_{l=0}^{4} c_l P_l(\cos\theta), \tag{4}$$

$$\sigma(\theta) T_{21}(\theta) = \frac{A_0}{2} \sum_{l=1}^{4} d_l P_l^1(\cos\theta), \tag{5}$$

$$\sigma(\theta) T_{22}(\theta) = \frac{A_0}{2} \sum_{l=2}^{4} e_l P_l^2(\cos\theta). \tag{6}$$

In these expressions $\sigma(\theta)$ is the unpolarized cross section and the P_l^m's are associated Legendre polynomials defined as in Ref. [12].

The solid curves in Fig. 2 show the best-fit Legendre expansion. The corresponding coefficients are listed in Table II, and the resulting total χ^2 is 15.1 (for 15 degrees of freedom). Table III contains a summary of which multipole combinations contribute to each expansion coefficients. From this table we see, for example, that the $l=0$ and $l=2$ coefficient (a_0, a_2, b_2, etc.) arise mainly from $E1 \cdot E1$ interference. From the results given in Tables II and III we can draw the following conclusions.

(1) The measured differential cross sections are consistent with expected dominance of the $S_c = \frac{1}{2}$ $E1$ transitions. If the two ^2P_j matrix elements are approximately equal in both magnitude and phase (as would be the case in plane-wave Born approximation) and the remaining transitions are small then one expects $a_2 \simeq -1$, as observed in the data.

(2) The fact that a_3 is nonzero is evidence for the existence of $E2$ radiation. In the cross section there is no interference between the $S_c = \frac{1}{2}$ and $S_c = \frac{3}{2}$ matrix elements, and thus we conclude that one or both of the ^2D_j matrix elements is nonzero. According to the measurements a_1 is approximately equal to $-a_3$. This observation can also be explained in a natural way assuming $E1 \cdot E2$ interference. In plane-wave Born approximation $[^2P_{1/2}]_{E1} = [^2P_{3/2}]_{E1}$ and $[^2D_{3/2}]_{E2} = [^2D_{5/2}]_{E2}$. If either of these conditions holds (and the $M1$ contributions are negligible) then $a_1 = -a_3$.

(3) As noted earlier, the tensor analyzing power measurements establish the existence of spin-flip transitions. Since the reaction is dominated by $S_c = \frac{1}{2}$, the observed analyzing powers presumably arise primarily from doublet-quartet interference. For the tensor analyzing powers only the $l=0$ and $l=2$ expansion coefficients are statistically nonzero, and therefore it is reasonable to conclude that these analyzing powers arise mainly from $E1 \cdot E1$ interference between the ^2P_j and the ^4P_j (or possibly $^4F_{3/2}$) amplitudes. Detailed matrix element fits, described below, indicate that both ^4P and ^4F must be present in order to simultaneously reproduce both T_{20} and T_{21} (if the $^4F_{3/2}$ matrix element is not included, the fits underestimate the magnitude of T_{21} by a significant amount).

(4) We turn next to the measurements of the vector analyzing powers, A_y and iT_{11}. One of the interesting points here is that nonzero values of b_2 and b_2' can arise from interference between the two dominant matrix elements, $[^2P_{1/2}]_{E1}$ and $[^2P_{3/2}]_{E1}$. In spite of this, the b_2 and b_2' coefficients are both quite small. If one retains only these two matrix elements then the expansion coefficients are given by

$$A_0 = \tfrac{1}{3} \{ |^2P_{1/2}|^2 + 2|^2P_{3/2}|^2 \}, \tag{7}$$

$$a_2 = -\tfrac{1}{3} \{ 2|^2P_{1/2}||^2P_{3/2}|\cos\phi + |^2P_{3/2}|^2 \} / A_0, \tag{8}$$

$$b_2' = -3b_2 = -\tfrac{1}{3} \{ |^2P_{1/2}||^2P_{3/2}|\sin\phi \} / A_0. \tag{9}$$

From these expressions one can see that the phase angle ϕ between the two ^2P_j matrix elements can be no more than

TABLE II. Best-fit Legendre expansion coefficients. The uncertainties in the last significant digits are given in parentheses.

l	σ a_l	A_y b_l	iT_{11} b_l'	T_{20} c_l	T_{21} d_l	T_{22} e_l
0	1.000			−0.020(3)		
1	0.187(5)	0.071(4)	−0.034(5)	−0.001(3)	−0.001(8)	
2	−0.970(6)	0.015(2)	−0.002(3)	0.015(6)	−0.044(4)	−0.006(3)
3	−0.178(10)	−0.001(2)	−0.001(2)	0.000(5)	−0.005(4)	−0.001(1)
4	−0.000(12)	−0.003(1)	−0.002(2)	0.009(8)	0.002(4)	0.001(1)

TABLE III. Multipole combinations contributing to each Legendre expansion coefficient.

l	Contributing multipoles
0	$\|E1\|^2+\|M1\|^2+\|E2\|^2$
1	$E1\cdot M1+E1\cdot E2$
2	$E1\cdot E1+M1\cdot M1+E2\cdot E2+M1\cdot E2$
3	$E1\cdot E2$
4	$E2\cdot E2$

a few degrees.

(5) The odd-l expansion coefficients can provide information about the even-parity matrix elements. We note that b_1 and b_1' are both nonzero, which requires the presence of either $M1$ or $E2$ radiation. We already know from the cross-section measurements that $E2$ radiation is present; however, it is unlikely that b_1 and b_1' arise from this source (it is possible for the $E2$ transitions to have no measurable effect on the vector analyzing powers if the $E1$ and $E2$ matrix elements have nearly equal phases). First of all, if b_1 and b_1' arise from $E1\cdot E2$ interference one would expect the $l=3$ coefficients to be nonzero as well, and this is not seen in the data. Second, the $E1$ and $E2$ contributions are both expected to be predominantly $S_c=\frac{1}{2}$. For pure doublet-doublet interference one obtains $b_l'=-3b_l$, and since this relationship does not hold true even approximately for the measured b_1 and b_1' coefficients, it seems unlikely that $E1\cdot E2$ interference is the source.

The most natural explanation is to assume that the observed b_1 and b_1' coefficients arise from $E1\cdot M1$ interference. If we again assume that the main source is interference with the $[^2P_j]_{E1}$ radiation, then for $S_c=\frac{1}{2}$ $M1$ contributions we obtain $b_l'=-3b_l$, while for $S_c=\frac{3}{2}$ $M1$ radiation the corresponding relationship as $b_l'=-\frac{3}{4}b_l$. The observed coefficients fall between the two limits, but are in fact quite close to the value expected for $S_c=\frac{3}{2}$ radiation. Thus, we take the measured b_1 and b_1' coefficients to be evidence for the existence of $S_c=\frac{3}{2}$ $M1$ radiation.

Using these conclusions as a guide, we have carried out a series of direct matrix-element fits of the data. Our goal here was to determine whether one can explain the measurements *quantitatively* using only a relatively small number of matrix element parameters. We find that a reasonable fit can be obtained by including all five $E1$ matrix elements along with the $[^2S_{1/2}]_{M1}$, $[^4S_{3/2}]_{M1}$, $[^2D_{3/2}]_{E2}$, and $[^2D_{5/2}]_{E2}$ matrix elements. In this fit the two $E2$ matrix elements are constrained to be equal. In addition, the $[^4F_{3/2}]_{E1}$ and the $[^2D_j]_{E2}$ matrix elements are constrained to be real (the overall phase is chosen so that the $[^2P_j]_{E1}$ matrix elements are, on average, real) and the $[^4S_{3/2}]_{M1}$ matrix element is constrained to be purely imaginary. The $[^2S_{1/2}]_{M1}$ matrix element is included since it allows a significant improvement in the fit both to the cross section and to the vector analyzing power measurements. The best fit (total $\chi^2=27.8$ for 28 degrees of freedom) is shown by the dashed curves in Fig. 2, and the corresponding matrix elements are listed in Table IV.

TABLE IV. Matrix elements obtained by fitting the measurements of Fig. 2. The results have been normalized to give $A_0=1$.

Matrix element	Multipolarity	Magnitude	Phase (deg)
$^2P_{1/2}$	$E1$	1.132	-0.3 [a]
$^2P_{3/2}$	$E1$	0.917	$+0.3$ [a]
$^4P_{1/2}$	Spin-flip $E1$	0.045	-39.1
$^4P_{3/2}$	Spin-flip $E1$	0.068	157.5
$^4F_{3/2}$	Spin-flip $E1$	0.025	180 [b]
$^2D_{3/2}$, $^2D_{5/2}$	$E2$	0.052	0 [b]
$^2S_{1/2}$	$M1$	0.051	163.7
$^4S_{3/2}$	$M1$	0.056	-90 [c]

[a]Phases constrained to be equal and opposite.
[b]Constrained to be real.
[c]Constrained to be imaginary.

In this fit the dominant $[^2P_j]_{E1}$ transitions account for approximately 99% of the total cross section, while the spin-flip $E1$ transitions, the $E2$ transitions, and the $M1$ transitions make up, respectively, 0.43%, 0.46%, and 0.30% of the total cross section. It should be noted, however, that the fit presented here is not unique. For example, an equally good fit can be obtained by using the $[^4D_{3/2}]_{M1}$ matrix element in place of $[^4S_{3/2}]_{M1}$. In addition, some of the matrix element parameters, specifically the real part of $[^4S_{3/2}]_{M1}$ and the imaginary parts of $[^4F_{3/2}]_{E1}$ and $[^2D_j]_{E2}$, are not well determined by the data and have been set to zero in the fit. Because of these ambiguities, the values quoted above for the $E2$, $M1$, and spin-flip $E1$ contributions should be considered lower limits.

Although many of the conclusions presented here have been known from previous work (see Refs. [4–11]), the new measurements are capable of placing much stronger constraints on the matrix elements (and more generally on theoretical calculations) than was previously possible. For example, the new data impose fairly strong constraints on the *individual* spin-flip $E1$ matrix elements. These transitions are of particular interest since they are thought to arise primarily from the D-state components of the ^{3}He wave function. In the past, efforts have been made to extract quantitative information about the ^{3}He D-state components from rather limited data sets (see Refs. [8, 10,11,14–17]). With our more extensive measurements, it should be possible to subject the various theoretical models to more rigorous scrutiny.

In summary, we have seen that the new measurements presented here are capable of providing a wealth of information about the nature of the p-d radiative capture reaction. We hope that these new data will stimulate further theoretical work, and that our detailed conclusions will serve as a useful guide for the theorists.

This work was supported in part by the National Science Foundation under Grant No. PHY-9019983.

[1] W. Haeberli, M. D. Barker, C. A. Gossett, D. G. Mavis, P. A. Quin, J. Sowinski, T. Wise, and H. F. Glavish, Nucl. Instrum. Methods **196**, 319 (1982).

[2] C. A. Gossett, Ph.D. thesis, University of Wisconsin, 1983, available from University Microfilms, Ann Arbor, MI 48106.

[3] F. Goeckner, Ph.D. thesis, University of Wisconsin, 1991, available from University Microfilms, Ann Arbor, MI 48106.

[4] D. M. Skopik, H. R. Weller, N. R. Roberson, and S. A. Wender, Phys. Rev. C **19**, 601 (1979).

[5] S. E. King, N. R. Roberson, H. R. Weller, and D. R. Tilley, Phys. Rev. C **30**, 21 (1984).

[6] S. E. King, N. R. Roberson, H. R. Weller, D. R. Tilley, H. P. Engelbert, H. Berg, E. Huttel, and G. Clausnitzer, Phys. Rev. C **30**, 1335 (1984).

[7] M. C. Vetterli, J. A. Kuehner, C. Bamber, N. Davis, A. J. Trudel, H. R. Weller, and R. M. Whitton, Phys. Rev. C **38**, 2503 (1988).

[8] W. K. Pitts *et al.*, Phys. Rev. C **37**, 1 (1988).

[9] M. Baumgartner, J. Jourdan, G. R. Plattner, W. D. Ramsay, H. R. Roser, and I. Sick (unpublished); see Ref. [15].

[10] M. C. Vetterli, J. A. Kuehner, A. J. Trudel, C. L. Woods, R. Dymarz, A. A. Pilt, and H. R. Weller, Phys. Rev. Lett. **54**, 1129 (1985).

[11] J. Jourdan *et al.*, Nucl. Phys. A **453**, 220 (1986).

[12] R. G. Seyler and H. R. Weller, Phys. Rev. C **20**, 453 (1979).

[13] S. Mellema, T. R. Wang, and W. Haeberli, Phys. Rev. C **34**, 2043 (1986).

[14] S. E. King, N. R. Roberson, H. R. Weller, and D. R. Tilley, Phys. Rev. Lett. **51**, 877 (1983).

[15] A. Arriaga and F. D. Santos, Phys. Rev. C **29**, 1945 (1984).

[16] J. L. Ballot and A. M. Eiro, Few-Body Systems, Suppl. 2, 389 (1987).

[17] A. C. Fonseca and D. R. Lehman, Phys. Lett. B **267**, 159 (1991).